



# Actuation and locomotion driven by moisture in paper made with natural pollen

Ze Zhao<sup>a,1</sup>, Youngkyu Hwang<sup>a,1</sup> , Yun Yang<sup>a</sup>, Tengfei Fan<sup>a</sup>, Juha Song<sup>b,2</sup> , Subra Suresh<sup>a,2</sup>, and Nam-Joon Cho<sup>a,2</sup>

<sup>a</sup>School of Materials Science and Engineering, Nanyang Technological University, 639798 Singapore, Singapore; and <sup>b</sup>School of Chemical and Biomedical Engineering, Nanyang Technological University, 637459 Singapore, Singapore

Contributed by Subra Suresh, February 26, 2020 (sent for review December 26, 2019; reviewed by Markus J. Buehler and Yonggang Huang)

**Here we describe the development of a humidity-responsive sheet of paper that is derived solely from natural pollen. Adaptive soft material components of the paper exhibit diverse and well-integrated responses to humidity that promote shape reconfiguration, actuation, and locomotion. This mechanically versatile and nonallergenic paper can generate a cyclically high contractile stress upon water absorption and desorption, and the rapid exchange of water drives locomotion due to hydrodynamic effects. Such dynamic behavior can be finely tuned by adjusting the structure and properties of the paper, including thickness, surface roughness, and processing conditions, analogous to those of classical soapmaking. We demonstrate that humidity-responsive paper-like actuators can mimic the blooming of the *Michelia* flower and perform self-propelled motion. Harnessing the material properties of bioinspired systems such as pollen paper opens the door to a wide range of sustainable, eco-friendly, and biocompatible material innovation platforms for applications in sensing, actuation, and locomotion.**

natural materials | biomimetics | pollen | actuators | wearable sensor

In natural ecosystems, many organisms dynamically interact with and mechanically adapt to the surrounding environment for specific biological functions (1–3). Examples include the opening of pine cones (4), the dispersion of wheat awn seeds (5), and the unfolding of ice plant seed capsules (6). At the molecular level, biological protein materials such as silk (7) and collagen (8) control their mechanical forces and motions by changing their molecular conformations in response to moisture. Inspiration drawn from such naturally occurring biological systems has led to the development of a wide range of artificial soft actuators that can reversibly alter morphological or mechanical characteristics in response to external stimuli (9–11). Owing to their dynamic responsiveness, these actuators have a wide range of potential applications, including soft robots (12–17), artificial muscles (18–21), sensors (22, 23), and electric generators (24, 25).

Significant progress has been made in the development of actuator materials. Consider, for example, the case of smart actuators wherein most of the key components are derived from graphene-based materials or synthetic polymers (26–30). Given the common limitations associated with these materials in terms of their relatively high cost, strict reaction control, and issues with environmental sustainability, the quest for more cost-effective materials from natural and renewable sources has accelerated (31–34). Although natural materials such as agarose (24, 32, 35) and cellulose (11, 36–38) are used in a number of applications, they must be extracted and refined from raw resources at a considerable energy cost. Furthermore, actuators constructed from some natural polymers typically exhibit a weak actuation response, and their dynamic response is typically not conducive to fabrication of components that demand cyclic variations in mechanical characteristics (39). In view of these considerations, it is highly desirable to explore the feasibility of development and widespread deployment of naturally abundant materials for applications requiring actuation and locomotion by recourse to eco-friendly, sustainable, and cost-effective processing and fabrication methods.

Here we describe a unique paper-like actuator made of a derivative of naturally occurring plant pollen, which is readily responsive to cyclic and reversible changes in humidity. Pollen grains are natural microparticles designed to encapsulate and transport plant genetic material and have been extensively studied owing to their practically indestructible structural characteristics (40). In particular, pollen grains are typically composed of two mechanically distinct layers: a tough sporopollenin exine and a soft cellulose intine (41–43). The double linkage of ester and acetal groups contributes to the superior mechanical stiffness and chemical inertness of the sporopollenin exine (44). Because of their toughness, pollens are also being explored for such applications as drug delivery microcapsules (45–48), reinforcing fillers (49), and micromotors (50). Importantly, pollen-derived microcapsules have been developed as nonallergenic carriers to harness such advantageous properties as high mechanical strength, chemical stability, UV protection, and pathogen inhibition (51, 52). Recently, we also demonstrated that it is possible to convert hard pollen grains into soft, stimuli-responsive microgel particles (53). However, the potential for developing other material forms based on natural, nonallergenic, and inexpensive pollen grains, thereby harnessing their unique functional capabilities and applications, has not been investigated to date.

## Significance

Much progress has been made in developing bioinspired sensors and actuators based on engineered synthetic materials, although there remains a critical need to incorporate cost-effective and eco-friendly materials. Here naturally abundant pollen grains are used as a material template to produce paper that sensitively and reversibly responds as an actuator to variations in environmental humidity. The actuating properties of the all-natural paper are readily tuned by material characteristics, such as sheet thickness and surface roughness. We demonstrate self-actuation of the pollen-based paper by mimicking flower blooming. The results presented here point to pathways for the creation of self-propelled robots, flexible electronics, and multifunctional devices. They also offer the potential for digital printing and fabrication of complex and programmable natural actuators.

Author contributions: Z.Z., Y.H., and N.-J.C. designed research; Z.Z., Y.H., Y.Y., and T.F. performed research; Z.Z., Y.H., Y.Y., J.S., S.S., and N.-J.C. analyzed data; and Z.Z., Y.H., J.S., S.S., and N.-J.C. wrote the paper.

Reviewers: M.J.B., Massachusetts Institute of Technology; and Y.H., Northwestern University.

Competing interest statement: N.-J.C. is an inventor on a related technology disclosure filed by Nanyang Technological (TD/300/17).

This open access article is distributed under [Creative Commons Attribution-NonCommercial-NoDerivatives License 4.0 \(CC BY-NC-ND\)](https://creativecommons.org/licenses/by-nc-nd/4.0/).

<sup>1</sup>Z.Z. and Y.H. contributed equally to this work.

<sup>2</sup>To whom correspondence may be addressed. Email: SSuresh@ntu.edu.sg, songjuha@ntu.edu.sg, or njcho@ntu.edu.sg.

This article contains supporting information online at <https://www.pnas.org/lookup/suppl/doi:10.1073/pnas.1922560117/-DCSupplemental>.

In this study, we demonstrate a method capable of preparing and transforming soft pollen microgels into a flexible and translucent 2D paper-like material. The simple drying process is attributed to the activity of the functional groups during hydrogen bond formation, whereby pollen particles are assembled into microscale building blocks. Surprisingly, the resulting pollen paper exhibits sensitive and reversible mechanical shape change and continuous locomotion in response to water vapor stimulation. This behavior arises from the naturally synergetic coupling between the hydro-expansion and water vapor barrier properties of pollen paper. The top and bottom surfaces of the paper can also be made to exhibit different degrees of responsiveness to moisture from differing and asymmetric microstructures, a feature rarely seen in other monocomponent actuation systems. The actuating power of pollen paper is also readily adjusted by modulating the paper thickness and/or the processing conditions.

Considering these mechanistic properties, we designed a device fabricated from pollen paper that mimics the blooming of the *Michelia* flower. By also making use of the high viscosity of soft pollen microgels, we developed a proof-of-concept walking robot. The results of this work thus point to the wide spectrum of possibilities for printing new classes of pollen-derived natural materials with complex shapes for programmable actuators.

## Results and Discussion

We began with a simple approach for the self-assembly of pollen grains from sunflower plants (*Helianthus annuus*) into a paper-like geometry. First, we transformed practically indestructible, ultra-tough, defatted pollen grains into pliable, soft hollow materials. Fig. 1A shows sunflower pollen grains of oval shape with spiky appendages on their surfaces. These grains preserve their original 3D shapes in dry and vacuum conditions, as shown by field emission scanning electron microscopy (FESEM). We softened the hard pollen grains using the traditional two-step soap-making process. This process involves pollen shell extraction and subsequent incubation in an alkaline medium, which in

this work was potassium hydroxide (KOH). Specifically, the defatted pollen was treated with 10 wt/vol% KOH at 80 °C and stirred for 2 h to remove its internal cytoplasmic content (Fig. 1B). Then it was statically incubated in fresh 10 wt/vol% KOH at 80 °C for specific periods of time (3, 6, or 12 h) to facilitate extensive hydrolysis that transforms hard pollen into mechanically weaker microgel particles. Subsequent neutralization and centrifugation yield stable pollen microgel suspensions, as shown in Fig. 1C.

In marked contrast to the original defatted pollen particles (30 μm in diameter), the pollen particles that had been incubated in KOH for 6 h swelled to 43 μm in diameter. These particles experienced significant structural collapse and flattening after natural drying, as shown in the FESEM image in Fig. 1C. Moreover, prolonged incubation in KOH led to a significant loss of mechanical stiffness, which facilitates swelling during hydration and flattening during dehydration (SI Appendix, Fig. S1). Because of the enhanced exposure of their functional groups during hydrolysis and owing to their softness and pliability, pollen microgels derived from plants are analogous to cellulose or lignin and can serve as potential building blocks for the fabrication of higher-order structural assemblies (54–56).

We used a conventional film-making strategy to assemble the pollen microgels, as shown in Fig. 1D. Dilute pollen microgels were easily cast into the desired mold (a Petri dish in this study). The concentration of pollen particles gradually increased with water evaporation, resulting in the agglomeration of particles and leading to continuous paper-like assemblies. Here the paper, which is constructed by λ-h KOH-incubated pollen microgels, is termed the λ-h sample accordingly.

The pollen paper exhibited excellent mechanical flexibility and two distinctly different surfaces: a frosted top surface that was exposed to air and a mirror-like bottom surface resulting from contact with the bottom of the mold during water evaporation (Fig. 2A). Fourier transform infrared (FTIR) spectroscopy was used to determine the molecular structural shift (SI Appendix, Fig. S2), which indicated enhanced exposure of functional

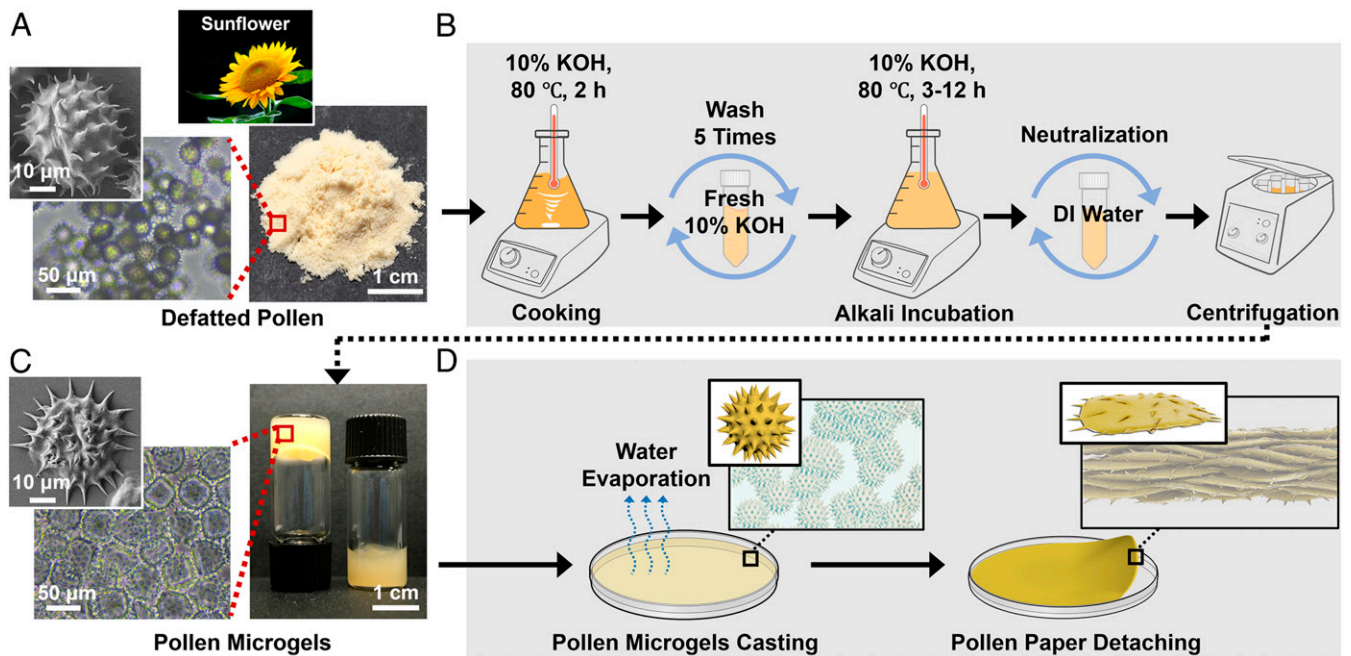


**Fig. 1.** Pollen paper prepared by alkali treatment of naturally derived pollen grains and subsequent casting. (A) Morphology and structure of defatted sunflower pollen shown at multiple length scales through optical and electron microscopy. (B) Steps in the preparation of pollen microgels. (C) Pollen microgels incubated in KOH for 6 h, shown at multiple length scales. (D) Schematic illustration of mold cast of pollen microgels for fabricating freestanding paper through water evaporation.

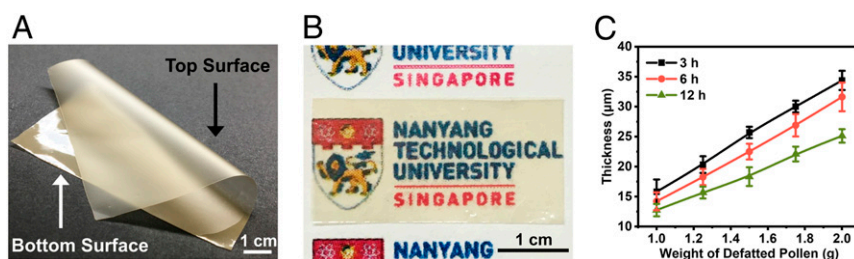


**Fig. 2.** Appearance and characteristics of paper derived from pollen microgels. (A) Image of a flexible pollen paper (6 cm × 6 cm) following complete drying of the cast pollen microgels incubated in KOH for 6 h. The black arrow indicates the frosted top surface of the paper, which was exposed to air during water evaporation. The white arrow indicates the mirror-like lower surface of the paper, which was in contact with the bottom of the Petri dish during water evaporation. (B) The pollen paper (1 cm × 2 cm) placed on top of an A4 size regular white paper printed with logos to illustrate the transparency of the former sample. (C) Thickness of 3-h, 6-h, and 12-h samples as a function of the weight of original defatted pollen grains.

groups active in the formation of hydrogen bonds between the pollen particle surfaces. Consequently, integrated and free-standing pollen paper could be obtained. Fig. 2B shows the high transparency of this pollen paper. Moreover, the thickness of the paper can be readily controlled by adjusting the weight of the original defatted pollen grains, and an increase in KOH incubation time leads to a decrease in thickness because of prolonged alkaline hydrolysis of pollen particles (Fig. 2C).

Differences in the macroscopic appearance of the surfaces of the pollen paper can be traced to their underlying microstructures. As shown in FESEM and atomic force microscopy (AFM) images (Fig. 3A and *SI Appendix*, Fig. S3), the top surface of the pollen paper had a nonuniform morphology and an apparent structure with remnants of features from the removed spikes, whereas the bottom surface was relatively much smoother (Fig. 3B and *SI Appendix*, Fig. S4). This finding was supported by an analysis of surface roughness using AFM, which revealed significant differences in roughness between the top and bottom surfaces irrespective of KOH incubation time. Furthermore, with an increase in incubation time, the roughness of the top surface decreased, whereas the bottom surfaces of all 3-h, 6-h, and 12-h samples exhibited nearly identical low surface roughness (Fig. 3C and *SI Appendix*, Fig. S5). In addition, a significant reduction in stiffness of the pollen paper was seen with an increase in KOH incubation time (Fig. 3D). This suggests increased softening of the pollen microgel particles with longer incubation time and further indicates a decrease in surface roughness (Fig. 3C). The laminated nature of the pollen paper is evident in the cross-sectional view seen under FESEM (Fig. 3E), from which the flat collapse and deposition of pollen particles were verified. Compared with the 3-h sample, the pollen papers that had an extended KOH incubation time exhibited a more compact and well-stacked multilayered structure (*SI Appendix*, Fig. S6).

The pollen paper absorbs water due to the exposure of hydrophilic functional groups during alkaline hydrolysis. The paper exhibited a unique water absorption behavior: when placed on a water surface, it rolled up quickly and sharply and then slowly unrolled (*Movie S1*). As a result, the surface area of the paper that had been moisture-soaked was dramatically enlarged, by more than ~80% in the 6-h sample, as shown in Fig. 4A. Changes in both surface area and weight before and after water absorption were measured, from which we determined that a longer KOH incubation time resulted in increases in both parameters (Fig. 4B and *SI Appendix*, Fig. S7). Given its lamellar structure and excellent swelling rate resulting from water absorption, the pollen paper appeared to exhibit a degree of mechanical responsiveness to humidity somewhat similar to that of many synthetic materials studied previously (14, 18, 22, 25).

The sensitivity of the pollen paper to moisture is illustrated with images from a simple experiment shown in Fig. 4C. When a square piece of the paper is held on a bare human palm, moisture

from sweat is absorbed by the paper and it curls up, developing a strong curvature. The reversibility of this deformation is also evident in the figure, when the same piece of paper quickly recovers its original flat surface when transferred to the dry surface of a palm covered with a rubber glove. To better understand this water absorption/desorption mechanism, we used FTIR spectroscopy to characterize the pollen paper after it had been in contact with D<sub>2</sub>O vapor to prevent any interference from ambient H<sub>2</sub>O. The results demonstrate that the vibration band of D<sub>2</sub>O (~2,500 cm<sup>-1</sup>) evolved only on the contact surface and not on the noncontact surface, which caused anisotropic swelling of the paper and activated its deformation (*SI Appendix*, Fig. S8). Water desorption of the pollen paper was also monitored by detecting the peak corresponding to the D<sub>2</sub>O band, ν(OD), at 2-min intervals. As shown in *SI Appendix*, Fig. S9, the paper exhibited the most intensive ν(OD) after saturated D<sub>2</sub>O absorption, which was followed by a rapid decline in the signal due to rapid desorption in low humidity conditions.

A schematic representation of the mechanistic processes driving this phenomenon is shown in Fig. 4D. Here the cross-section of the pollen paper is depicted as a layered structure (represented by orange-colored flat ellipses), somewhat analogous to the laminated microarchitecture shown in Fig. 3E. Asymmetrical exposure to water vapor induces stronger interaction of hydrogen bonds between the water molecules and the surfaces of pollen particles. The ensuing weakening of the original hydrogen bonds between the pollen particles leads to expansion of the spaces between the pollen particles. Closely packed and layered pollen particles, tens of micrometers in thickness, act as barriers to hinder and delay the diffusion of water molecules. This unique structure arising from the differential swelling of pollen paper induces internal stresses through the thickness of the paper, which forces it to bend. As the water vapor is removed, the hydrogen bonds between the pollen particles strengthen, forcing the paper to return to its original, mechanically unbent state.

Continuous absorption of water leads to the pollen paper ultimately reaching an equilibrium point beyond which it cannot adsorb any more water at a given relative humidity (RH) level. Any variation in RH can easily shift the equilibrium or saturation point and thereby reversibly change the weight of the paper, as shown in Fig. 5A. In addition to the weight change, variation in RH also has a strong effect on the mechanical properties of the pollen paper. Taking the 6-h sample as an example, the paper has a much lower Young's modulus ( $E = 0.66$  GPa) and a higher elongation to failure (44%) at 60% RH than at 20% RH (1.46 GPa and 7.6%, respectively) (*SI Appendix*, Fig. S10). This suggests that moisture weakens the connections between pollen particles, and that the mechanical properties of the pollen paper are also strongly influenced by humidity.

Fig. 5B shows the experimental setup in which a small strip of pollen paper (20 mm × 5 mm) was subjected to a fixed tensile strain

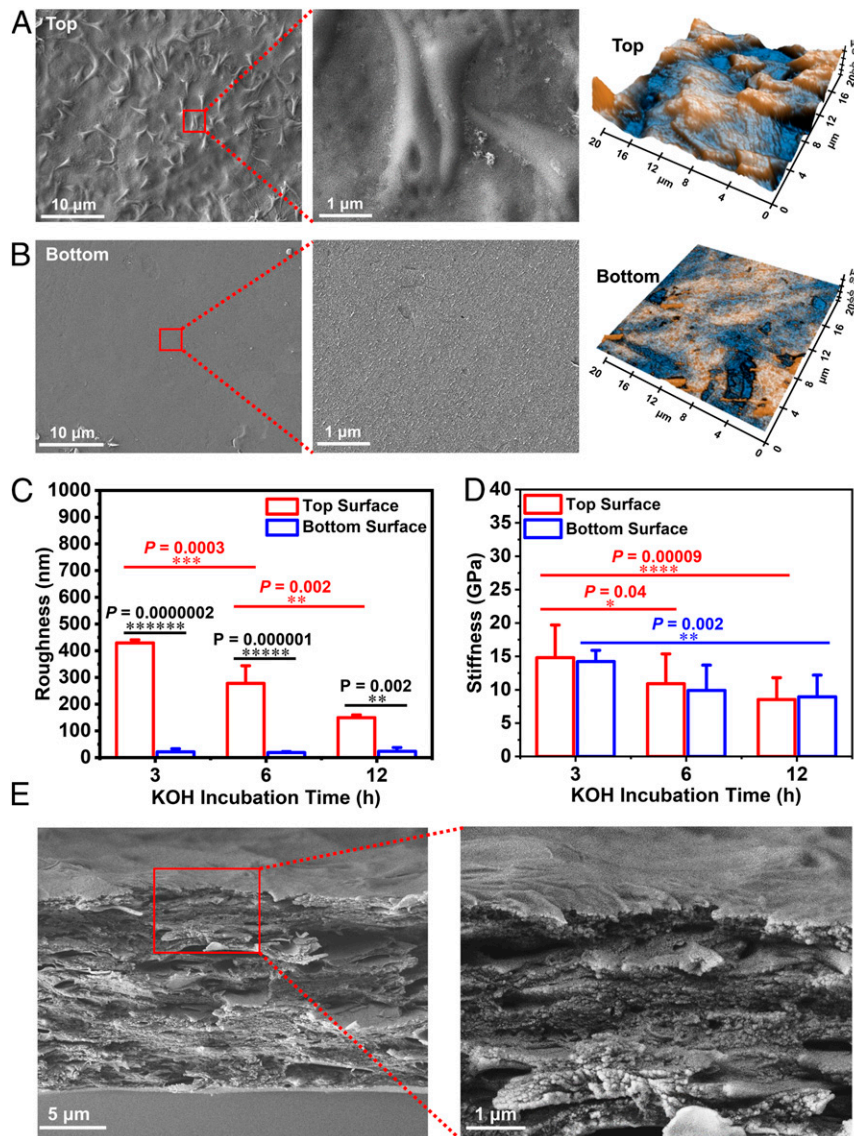


**Fig. 3.** Microstructures and micromorphology of pollen papers. (A and B, Left) FESEM images of top surface (A) and bottom surface (B) of 6-h samples at low and high magnifications. (A and B, Right) AFM images of the top and bottom surfaces of 6-h samples. (C and D) Roughness (C) and stiffness (D) of top and bottom surfaces of 3-h, 6-h, and 12-h samples measured by AFM. The error bars are obtained from the SDs generated by 10 duplicate tests. (E) SEM images of the cross-section of 6-h samples at low and high magnifications. (Scale bars: 5  $\mu\text{m}$  at low magnification; 1  $\mu\text{m}$  at high magnification.)

of 1%. This deformation required tensile stress of  $\sim 2$  MPa under humid conditions at 60% RH. When RH was decreased from 60% to 20%, contractile stresses were generated within the sample, and in turn the imposed tensile stresses had to be raised to 6.6 MPa to maintain the tensile strain of 1%. Based on its obvious hygro-mechanical responsiveness and good reversibility, when placed on a flat nylon mesh above a water bath, the pollen paper (specimen size, 2 cm  $\times$  2 cm) was observed to undergo a spontaneous and continuous flipping locomotion cycle, as shown in Fig. 5C and Movie S2. When exposed to a gradient in humidity level, the bottom-facing surface expanded more than the opposite surface (i.e., the top-facing surface). This differential expansion caused the paper to curl up. Finally, the pollen paper unrolled upside down and then curled up from the other perpendicular sides to start a new cycle because of its hygro-mechanical reversibility. Fig. 5D shows a schematic illustration of one complete cycle. A longer KOH incubation time produced a more pronounced increase in the flipping locomotion speed (Movie S2).

Key factors in the development of stimuli-responsive materials entail controllability and tunability of shape, deformation, and locomotion in a reversible manner. For the present pollen paper, there exists considerable design flexibility to modulate these key factors by recourse to the selection of KOH incubation time, in addition to tailoring geometrical variables such as the thickness of the paper. Moreover, the asymmetric microtopographies of the top and bottom surfaces lead to different levels of mechanical response due to different levels of exposure to water (Fig. 3 A and B).

We next demonstrated mechanical actuation in pollen paper through the control of such factors as KOH incubation time and paper thickness. For this purpose, we designed a simple apparatus comprising a metal mesh and a beaker containing water that can create a humidity difference of  $\sim 20\%$  between the metal surface (RH  $\sim 70\%$ ) and the ambient environment (RH  $\sim 50\%$ ), as shown in Fig. 6A. The paper specimen (1 cm  $\times$  1 cm) was positioned on the metal mesh with only one side fixed and could be exposed to and shielded from the water vapor by horizontally

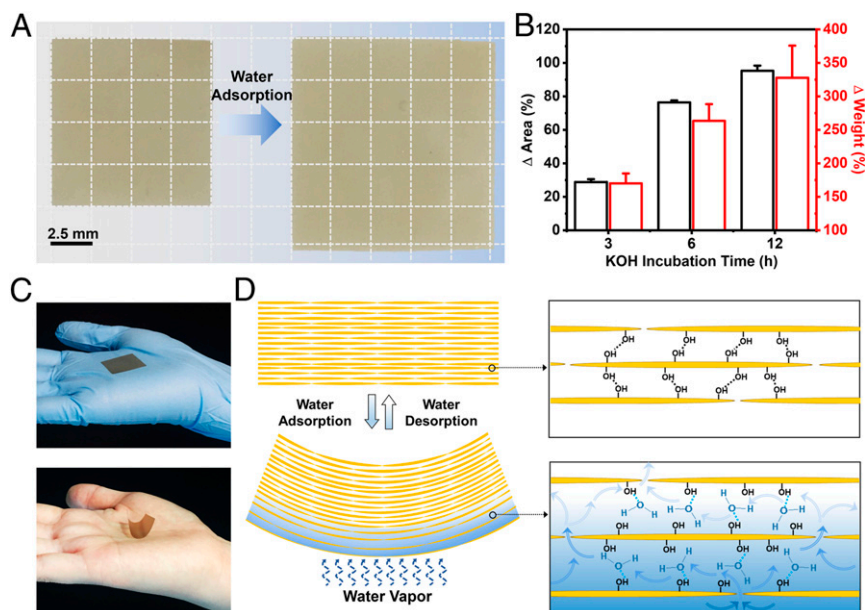


**Fig. 4.** Demonstration of the sensitive and reversible response of pollen paper to humidity. (A) Change in size of the paper before and after saturated water absorption. (B) Area and weight changes of paper as a function of KOH incubation time on complete water absorption following immersion in deionized water for 1 h. (C) A square sheet of pollen paper exhibited different behavior from human sweat when placed on the palm with and without gloves. (D) Schematic representation of the chemistry-mediated bending of the paper triggered by water vapor.

moving the metal mesh. When moved to a position above the water, the paper curved up until it reached a steady state. During this process, the evolution of the bending angles was recorded, and the resulting curvature,  $\kappa$ , was estimated.

The KOH incubation time was investigated for a fixed paper thickness of  $27\ \mu\text{m}$ . As shown in Fig. 6B, when positioned with the top surface facing the water, the 6-h and 12-h samples showed similar bending kinetics, which were faster than those of the 3-h samples. All of the samples exhibited a steady-state curvature within  $\sim 80\ \text{s}$ . As the KOH incubation time increased, the steady-state curvature increased from  $1.2\ \text{cm}^{-1}$  to  $1.9\ \text{cm}^{-1}$  due to enhanced water absorption (Fig. 6C). When the paper samples were moved away from water, the 3-h, 6-h, and

12-h samples returned to their unbent flat state within approximately 20 s, 40 s, and 60 s, respectively (SI Appendix, Fig. S11A). Interestingly, when the paper sheets were turned over so that the bottom surfaces faced the water, three samples displayed comparable bending and relaxation kinetics, and all exhibited faster bending and unbending speeds than were seen when the top surface was facing the water (Fig. 6D and SI Appendix, Fig. S11B). We interpret this differential behavior by noting that the smoother and more compact bottom layers of pollen paper demonstrate a greater propensity to hinder the diffusion of water molecules compared with the top layers. The result is an acceleration in the establishment of moisture equilibrium throughout the paper, which leads to larger differences in the degree of

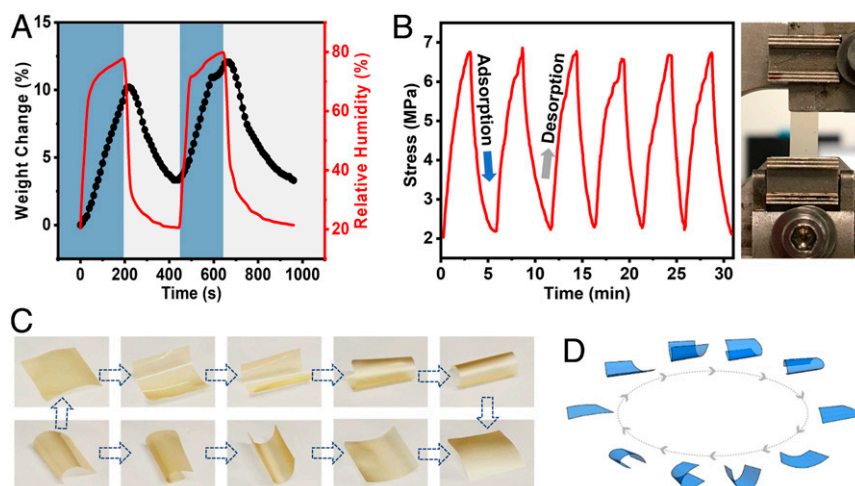


**Fig. 5.** Demonstration of the sensitive and reversible response of pollen paper to humidity. (A) Variation in the weight of pollen paper sheet with respect to a change in the surrounding RH. (B) The contractile stress generated in pollen paper on water desorption. The photo on the right shows a clamped pollen paper sheet subjected to a fixed strain under tension while the variations in tensile stress due to moisture absorption and desorption were measured in several repeated cycles at RH levels fluctuating between 60% and 20%. (C and D) Representative images (C) and schematic diagram (D) of the multistage locomotion of the paper when placed on a nylon mesh at a distance of 5 mm above the surface of a water bath.

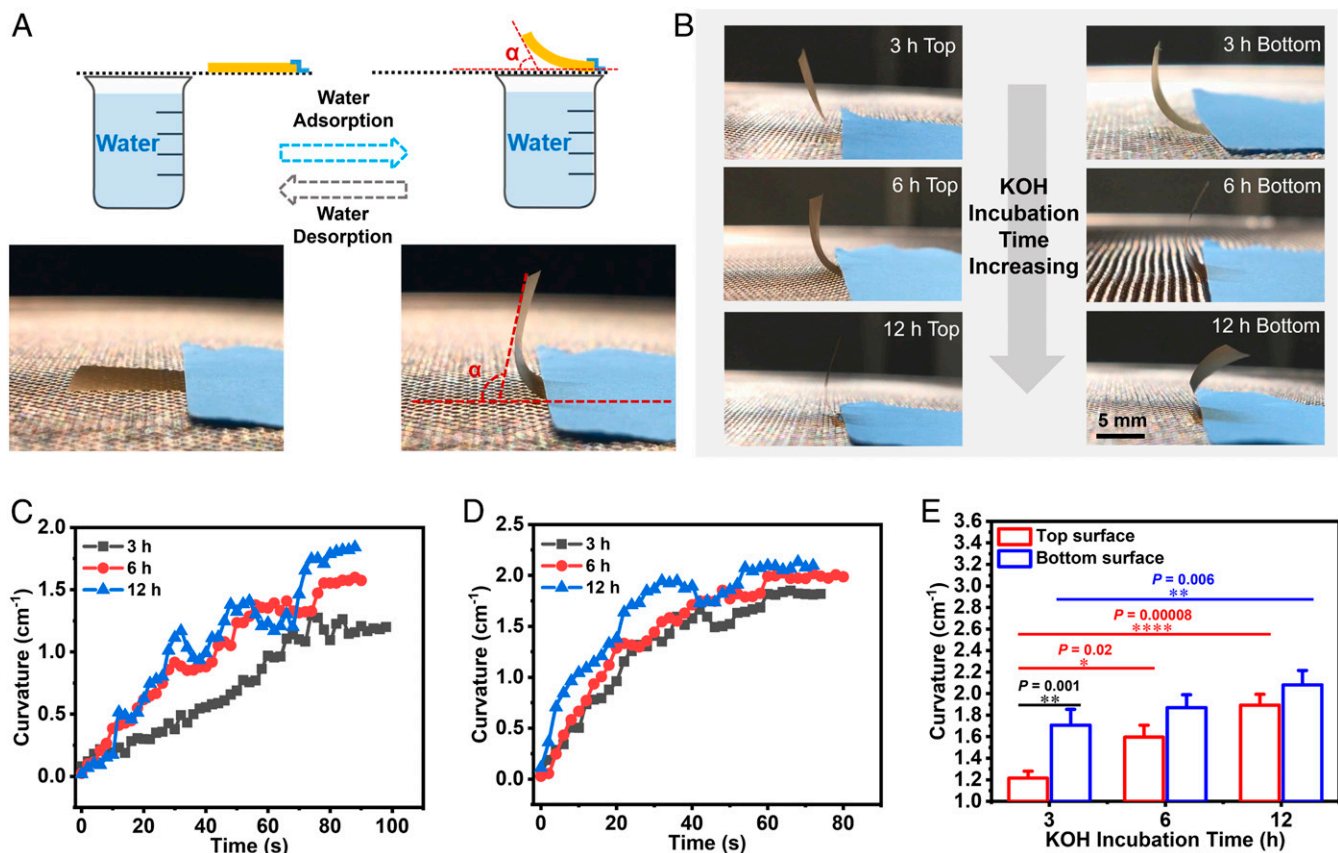


**Fig. 6.** Experimental demonstration of the tunability of actuation under controlled humidity conditions and through selection of KOH incubation time. (A, Top) Schematic diagram of the quantitative measurement of paper deformation and the resultant curvature. This was accomplished by fixing one side of the paper (1 cm × 1 cm) to a metal mesh above a water bath, which provides a relatively fixed humidity gradient of 20%. Curvature,  $\kappa = \pi\alpha/(180^\circ L)$ , where  $\alpha$  is the deflection angle and  $L$  is the paper length (in this case 1 cm). (A, Bottom) Photos of pollen paper fixed at one end under hydrated and dehydrated states by the absorption and desorption of water vapor, respectively. (B) Photos of hydrated pollen papers (thickness 27  $\mu\text{m}$ ) showing that the steady-state bending angles increased as the KOH incubation time increased for both the top and bottom surfaces. (C and D) Bending kinetics showing curvature evolution as a function of time for the pollen papers fabricated with different KOH-incubated pollen microgels when the top surface (C) or bottom surface (D) was exposed to water vapor. (E) Characterization of steady-state curvatures as a function of KOH incubation time.

swelling and evolution of internal stress between the two sides of the paper. As a result, compared with the top surface, the bottom surface generally exhibited increased curvature, as shown in Fig. 6E. Furthermore, these differences in responsiveness between the top and bottom surfaces became smaller as the KOH incubation time increased, due to the decreasing difference in roughness between their top and bottom surfaces. Moreover, an increased paper thickness was observed to slow bending kinetics and decrease steady-state curvatures (SI Appendix, Figs. S12 and S13).

We next demonstrate the potential application of pollen paper as a self-actuating soft robot. For this purpose, we designed a biomimetic *Michelia* flower (Fig. 7A and SI Appendix, Fig. S14A). After insertion into a vial full of water, the biomimetic flower continued to bloom from the gradual absorption of water vapor that had been absorbed by the sponge from the vial (Fig. 7B and SI Appendix, S14B) within 100 s, as shown in Movie S3.

Pollen paper sheets incubated in KOH for different periods (e.g., 3 h vs. 12 h) exhibit different responses to humidity-mediated actuation, theoretically making it possible to tailor specific mechanical actuation and locomotion behaviors in pollen paper by recourse to careful choices of paper samples prepared under different KOH incubation times. To test this hypothesis, we fabricated a simple binary pollen strip capable of unidirectional walking under cyclic variations in humidity, as shown in Fig. 7C. In this experiment, 3-h and 12-h pollen microgel samples, each with a volume of 200  $\mu\text{L}$ , were placed onto the surface of a Petri dish,

which was hydrophobic (SI Appendix, Fig. S15A). Due to their gel-like physical properties, the two pollen microgels did not diffuse into one another, which led to a visible mechanical interface at their junction. The 12-h pollen microgels contained fewer pollen particles than the 3-h sample per unit volume, which could also spread to a larger area on the hydrophobic surface on demand because of its higher viscosity (SI Appendix, Fig. S15B). As a result, a thinner area was obtained in the 12-h section (13.45  $\mu\text{m}$ ) compared with the 3-h section (46.63  $\mu\text{m}$ ) (Fig. 7C, red and blue frames). At the interface, a strong mechanical boundary was observed (Fig. 7C, green dotted frame). When the bimaterial pollen strip was exposed to cyclic variations in humidity gradients, unidirectional movement of the biomaterial strip was observed (Fig. 7D and Movie S4). Fig. 7E shows the walking mechanism. At the beginning of the experiment, the pollen strip remained flat due to its uniform absorption of water from the surrounding high humidity. A subsequent decrease in humidity from below caused the 12-h section to bend inward and dramatically drag the left edge toward the right. Conversely, due to its lesser hygroscopic expansion and greater thickness, the 3-h section showed only negligible bending behavior, and the right edge remained stationary. When high humidity was reintroduced, the 12-h section adsorbed water and flattened again. At that moment, the left-edge experienced greater friction because of the larger contact angle with respect to the substrate compared with that of the right edge,

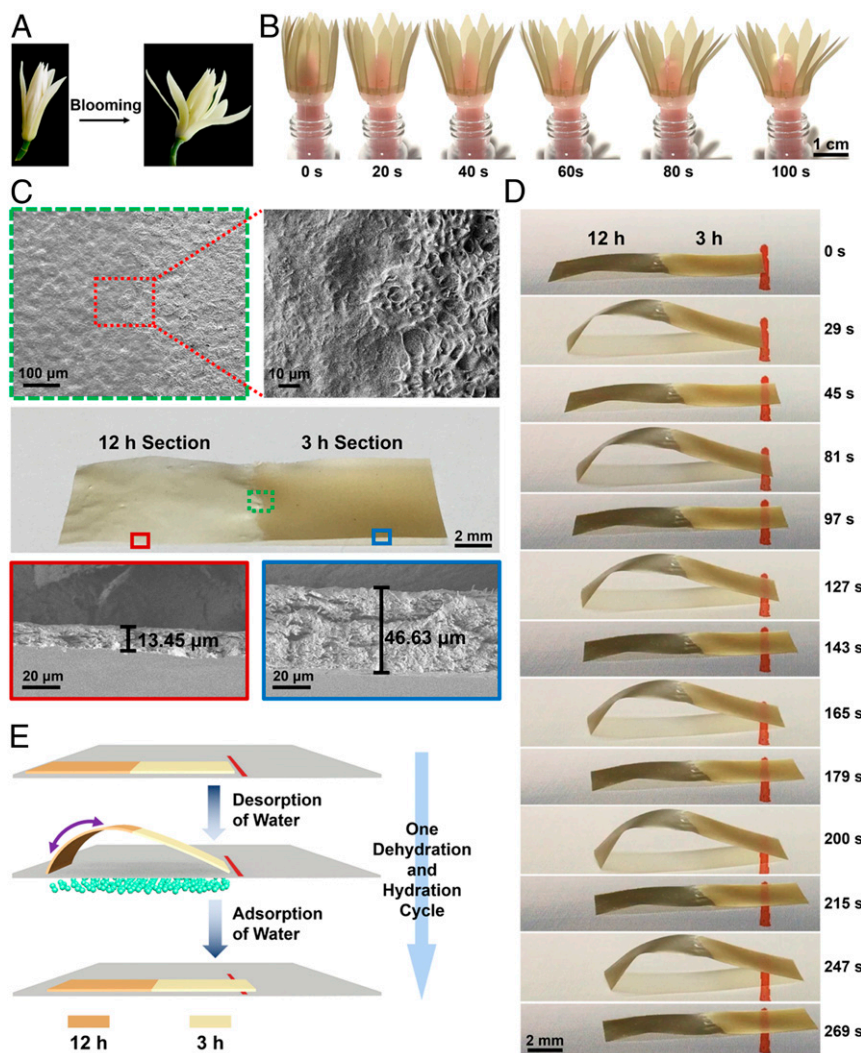


**Fig. 7.** Biomimetic application of the pollen paper actuator. (A) Blooming of *Michelia* flower. (B) Blooming of the biomimetic flower after insertion into a vial with water. (C) An image of the biomimetic walking robot in a dried state, which was designed by combining 12-h and 3-h KOH-incubated samples. (Top) SEM images showing the interface between the two sections at low and high magnifications. (Bottom) SEM images showing cross-sectional views of the 12-h and 3-h sections. (D) Images of the walking motion of the pollen paper robot in response to alternating low/high cycles of humidity. (E) Schematic illustration of the walking motion in one cycle.

which caused the right edge to move right during the unbending of the 12-h section. This caused the pollen strip to move to the right.

In summary, using eco-friendly treatment of naturally occurring pollen that is rendered nonallergenic through a simple fabrication process, we have created an economically viable soft actuator with a highly sensitive response to water vapor. The transformed hollow pollen microgel particles serve as pliable and collapsible building blocks that could self-assemble into papers. With its significant hydro-expansion capability and laminated microstructure, the pollen paper exhibits strong mechanical actuation under changing conditions of humidity, which could be easily tailored for specific applications by varying the paper thickness and KOH incubation time in the paper fabrication step. Notably, a difference in the degree of responsiveness between the top and bottom surfaces was noted. To demonstrate the potential of this work to a broad variety of applications, a bioinspired blooming flower was successfully fabricated.

Furthermore, taking advantage of the high viscosity of pollen microgels, we designed a walking robot comprising two pollen sections composed of different KOH-incubated pollen microgels. This pollen actuator demonstrates the potential for developing a wide spectrum of smart and eco-friendly actuation systems with tunable properties that dynamically respond to different functional needs.

**Data Availability.** Data supporting the findings of this study are available in the main text and *SI Appendix*. Additional information is available from the corresponding authors on reasonable request.

**ACKNOWLEDGMENTS.** This work was supported by the National Research Foundation of Singapore through a Competitive Research Program grant (NRF-CRP10-2012-07) and by Agency for Science, Technology and Research (A\*STAR) through the A\*STAR Advanced Manufacturing and Engineering Individual Research Grants (AME IRG) (A1983c0031). S.S. acknowledges support from Nanyang Technological University, Singapore, through a Distinguished University Professorship.

1. S. Armon, E. Efrati, R. Kupferman, E. Sharon, Geometry and mechanics in the opening of chiral seed pods. *Science* **333**, 1726–1730 (2011).
2. P. Chen *et al.*, Hierarchically arranged helical fibre actuators driven by solvents and vapours. *Nat. Nanotechnol.* **10**, 1077–1083 (2015).

3. P. Fratzl, F. G. Barth, Biomaterial systems for mechanosensing and actuation. *Nature* **462**, 442–448 (2009).
4. C. Dawson, J. F. V. Vincent, A.-M. Rocca, How pine cones open. *Nature* **390**, 668 (1997).

5. R. Elbaum, L. Zaltzman, I. Burgert, P. Fratzl, The role of wheat awns in the seed dispersal unit. *Science* **316**, 884–886 (2007).
6. M. J. Harrington *et al.*, Origami-like unfolding of hydro-actuated ice plant seed capsules. *Nat. Commun.* **2**, 337 (2011).
7. D. Liu *et al.*, Spider dragline silk as torsional actuator driven by humidity. *Sci. Adv.* **5**, e9183 (2019).
8. A. Masic *et al.*, Osmotic pressure induced tensile forces in tendon collagen. *Nat. Commun.* **6**, 5942 (2015).
9. A. R. Studart, Biologically inspired dynamic material systems. *Angew. Chem. Int. Ed. Engl.* **54**, 3400–3416 (2015).
10. R. M. Erb, J. S. Sander, R. Grisch, A. R. Studart, Self-shaping composites with programmable bioinspired microstructures. *Nat. Commun.* **4**, 1712 (2013).
11. Q. Zhu, Y. Jin, W. Wang, G. Sun, D. Wang, Bio-inspired smart moisture actuators based on nano-scale cellulose materials and porous, hydrophilic EVOH nanofibrous membranes. *ACS Appl. Mater. Interfaces* **11**, 1440–1448 (2019).
12. L. Zhang *et al.*, Water-evaporation-powered fast actuators with multimodal motion based on robust nacre-mimetic composite film. *ACS Appl. Mater. Interfaces* **11**, 12890–12897 (2019).
13. Y. Liu *et al.*, Humidity- and photo-induced mechanical actuation of cross-linked liquid crystal polymers. *Adv. Mater.* **29**, 1604792 (2017).
14. O. M. Wani, R. Verpaalen, H. Zeng, A. Priimagi, A. P. H. J. Schenning, An artificial nocturnal flower via humidity-gated photoactuation in liquid crystal networks. *Adv. Mater.* **31**, e1805985 (2019).
15. H. Okuzaki, T. Kuwabara, K. Funasaka, T. Saido, Humidity-sensitive polypyrrole films for electro-active polymer actuators. *Adv. Funct. Mater.* **23**, 4400–4407 (2013).
16. H. Arzoo *et al.*, An autonomous actuator driven by fluctuations in ambient humidity. *Nat. Mater.* **15**, 1084–1089 (2016).
17. M. Schaffner *et al.*, 3D printing of robotic soft actuators with programmable bio-inspired architectures. *Nat. Commun.* **9**, 878 (2018).
18. J. He *et al.*, Highly efficient actuator of graphene/polydopamine uniform composite thin film driven by moisture gradients. *Adv. Mater. Interfaces* **3**, 1600169 (2016).
19. I. H. Tseng, J.-J. Li, P.-Y. Chang, Mimosa pudica leaf-like rapid movement and actuation of organosoluble polyimide blending with sulfonated polyaniline. *Adv. Mater. Interfaces* **4**, 1600901 (2017).
20. Y. Ge *et al.*, A bio-inspired homogeneous graphene oxide actuator driven by moisture gradients. *Chem. Commun. (Camb.)* **54**, 3126–3129 (2018).
21. Y. Zhang *et al.*, Graphene oxide-based moisture-responsive biomimetic film actuators with nacre-like layered structures. *J. Mater. Chem. A Mater. Energy Sustain.* **5**, 14604–14610 (2017).
22. R. Castaldo *et al.*, Humidity-driven mechanical and electrical response of graphene/cloisite hybrid films. *Adv. Funct. Mater.* **29**, 1807744 (2018).
23. J. Zhou, C. Wu, D. Wu, Q. Wang, Y. Chen, Humidity-sensitive polymer xerogel actuators prepared by biaxial pre-stretching and drying. *Chem. Commun. (Camb.)* **54**, 11610–11613 (2018).
24. L. Zhang, P. Naumov, Light- and humidity-induced motion of an acidochromic film. *Angew. Chem. Int. Ed. Engl.* **54**, 8642–8647 (2015).
25. N. A. Carter, T. Z. Grove, Protein self-assemblies that can generate, hold, and discharge electric potential in response to changes in relative humidity. *J. Am. Chem. Soc.* **140**, 7144–7151 (2018).
26. M. Y. Ji, N. Jiang, J. Chang, J. Q. Sun, Near-infrared light-driven, highly efficient bilayer actuators based on polydopamine-modified reduced graphene oxide. *Adv. Funct. Mater.* **24**, 5412–5419 (2014).
27. M. Weng *et al.*, Multiresponsive bidirectional bending actuators fabricated by a pencil-on-paper method. *Adv. Funct. Mater.* **26**, 7244–7253 (2016).
28. L. Zhang, P. Naumov, X. Du, Z. Hu, J. Wang, Vapomechanically responsive motion of microchannel-programmed actuators. *Adv. Mater.* **29**, 1702231 (2017).
29. B. Li, T. Du, B. Yu, J. van der Gucht, F. Zhou, Caterpillar-inspired design and fabrication of a self-walking actuator with anisotropy, gradient, and instant response. *Small* **11**, 3494–3501 (2015).
30. Y. L. Zhang *et al.*, Quantum-confined superfluidics-enabled moisture actuation based on unilaterally structured graphene oxide papers. *Adv. Mater.* **31**, e1901585 (2019).
31. N. Kannan, D. Vakeesan, Solar energy for future world: A review. *Renew. Sustain. Energy Rev.* **62**, 1092–1105 (2016).
32. L. Zhang, H. Liang, J. Jacob, P. Naumov, Photogated humidity-driven motility. *Nat. Commun.* **6**, 7429 (2015).
33. M. Ma, L. Guo, D. G. Anderson, R. Langer, Bio-inspired polymer composite actuator and generator driven by water gradients. *Science* **339**, 186–189 (2013).
34. J. Troyano, A. Carné-Sánchez, D. Maspocho, Programmable self-assembling 3D architectures generated by patterning of swellable MOF-based composite films. *Adv. Mater.* **31**, e1808235 (2019).
35. L. Zhang, S. Chizhik, Y. Wen, P. Naumov, Directed motility of hygroresponsive biomimetic actuators. *Adv. Funct. Mater.* **26**, 1040–1053 (2016).
36. C. Echeverria, L. E. Aguirre, E. G. Merino, P. L. Almeida, M. H. Godinho, Carbon nanotubes as reinforcement of cellulose liquid crystalline-responsive networks. *ACS Appl. Mater. Interfaces* **7**, 21005–21009 (2015).
37. P. Bettotti *et al.*, Dynamics of hydration of nanocellulose films. *Adv. Mater. Interfaces* **3**, 1500415 (2016).
38. K. Zhang *et al.*, Moisture-responsive films of cellulose stearoyl esters showing reversible shape transitions. *Sci. Rep.* **5**, 11011 (2015).
39. M. Wang, X. Tian, R. H. A. Ras, O. Ikkala, Sensitive humidity-driven reversible and bidirectional bending of nanocellulose thin films as bio-inspired actuation. *Adv. Mater. Interfaces* **2**, 1500080 (2015).
40. H. J. B. Birks, H. H. Birks, B. Ammann, The fourth dimension of vegetation. *Science* **354**, 412–413 (2016).
41. A. Diego-Taboada, S. T. Beckett, S. L. Atkin, G. Mackenzie, Hollow pollen shells to enhance drug delivery. *Pharmaceutics* **6**, 80–96 (2014).
42. A. F. Edlund, R. Swanson, D. Preuss, Pollen and stigma structure and function: The role of diversity in pollination. *Plant Cell* **16** (suppl.), S84–S97 (2004).
43. P. Gonzalez-Cruz, M. J. Uddin, S. U. Atwe, N. Abidi, H. S. Gill, A chemical treatment method for obtaining clean and intact pollen shells of different species. *ACS Biomater. Sci. Eng.* **4**, 2319–2329 (2018).
44. F. S. Li, P. Phyo, J. Jacobowitz, M. Hong, J. K. Weng, The molecular structure of plant sporopollenin. *Nat. Plants* **5**, 41–46 (2019).
45. R. C. Mundargi *et al.*, Lycoperidium spores: A naturally manufactured, superrobust biomaterial for drug delivery. *Adv. Funct. Mater.* **26**, 487–497 (2016).
46. M. G. Potroz *et al.*, Plant-based hollow microcapsules for oral delivery applications: Toward optimized loading and controlled release. *Adv. Funct. Mater.* **27**, 1700270 (2017).
47. R. C. Mundargi *et al.*, Natural sunflower pollen as a drug delivery vehicle. *Small* **12**, 1167–1173 (2016).
48. M. J. Uddin, H. S. Gill, From allergen to oral vaccine carrier: A new face of ragweed pollen. *Int. J. Pharm.* **545**, 286–294 (2018).
49. O. O. Fadiran, J. C. Meredith, Surface treated pollen performance as a renewable reinforcing filler for poly(vinyl acetate). *J. Mater. Chem. A* **2**, 17031–17040 (2014).
50. H. Wang *et al.*, Bioinspired spiky micromotors based on sporopollenin exine capsules. *Adv. Funct. Mater.* **27**, 1702338 (2017).
51. C. S. Bailey *et al.*, A natural solution to photoprotection and isolation of the potent polyene antibiotic, marinomycin A. *Chem. Sci. (Camb.)* **10**, 7549–7553 (2019).
52. M. Kaya *et al.*, Incorporation of sporopollenin enhances acid-base durability, hydrophobicity, and mechanical, antifungal and antioxidant properties of chitosan films. *J. Ind. Eng. Chem.* **47**, 236–245 (2017).
53. T.-F. Fan *et al.*, Transformation of hard pollen into soft matter. *Nat. Commun.* **11**, 1449 (2020).
54. D. Klemm *et al.*, Nanocelluloses: A new family of nature-based materials. *Angew. Chem. Int. Ed. Engl.* **50**, 5438–5466 (2011).
55. Y. Liu, Strong and flexible nanocomposites of carboxylated cellulose nanofibril dispersed by industrial lignin. *ACS Sustain. Chem. & Eng.* **6**, 5524–5532 (2018).
56. M. Farooq, T. Zou, G. Riviere, M. H. Sipponen, M. Österberg, Strong, ductile, and waterproof cellulose nanofibril composite films with colloidal lignin particles. *Biomacromolecules* **20**, 693–704 (2019).